Available online at www.sciencedirect.com
ScienceDirect
Journal of Catalysis 256 (2008) 24–36
JOURNAL OF CATALYSIS
www.elsevier.com/locate/jcat

Decomposition of methanol by Pd, Co, and bimetallic Co–Pd catalysts: A combined study of well-defined systems under ambient and UHV conditions

H. Borchert [a], B. Jürgens [a], T. Nowitzki [a], P. Behrend [b], Yu. Borchert [a], V. Zielasek [a], S. Giorgio [c], C.R. Henry [c], M. Bäumer [a,*]

[a] *University of Bremen, Institute of Applied and Physical Chemistry, 28359 Bremen, Germany*
[b] *University of Bremen, Center for Environmental Research & Technology (UFT), 28359 Bremen, Germany*
[c] *CRMCN-CNRS, Campus de Luminy, Case 913, 13288 Marseille Cédex 9, France* [1]

Received 5 October 2007; revised 17 February 2008; accepted 20 February 2008

Available online 9 April 2008

Abstract

We investigated the decomposition of methanol over Pd-based catalysts and the influence of Co as a second metal. To obtain mechanistic information on the reaction, we prepared structurally well-defined systems for studies in the ambient pressure regime and systems suitable for UHV studies in a dual approach. For the ambient pressure regime, monometallic and bimetallic Co/Pd nanoparticles supported on MgO were prepared by a wet-chemical method. FTIR spectroscopy was used to analyze the surface species that formed on the catalysts in the interaction with methanol, and the catalytic performance was studied in continuous-flow reactors. We found that methanol is dehydrogenated to CO already at room temperature by the Pd and Pd–Co catalysts, but high steady-state conversion requires temperatures above ∼150 °C. As could be shown by parallel studies of methanol decomposition on model catalysts prepared by physical vapor deposition under UHV conditions, CO desorption is the limiting factor at lower temperature. Pure Pd catalysts were found to be more active for methanol decomposition than the bimetallic Co–Pd catalysts. Although electronic effects in the bimetallic system facilitate desorption of CO at low temperature, this cannot compensate for the lower intrinsic activity of Co sites. We also investigated the influence of small amounts of oxygen on the decomposition of methanol. The activity of the Me/MgO catalysts was found to be higher in the presence of oxygen than in the absence of oxygen. Oxygen facilitates the removal of carbon species resulting from the C–O bond scission reaction channel.

Keywords: Palladium; Cobalt; Bimetallic catalysts; Methanol decomposition

1. Introduction

Decomposition as well as steam-reforming of methanol attracts increasing attention because of the possibility of using methanol as an on-board source of hydrogen for fuel cells and, in the case of methanol decomposition, of synthesis gas well [1]. Supported Pd particles have been found to be effective catalysts for both of the processes (reactions (1) and (2)) [1–6], which usually can occur in parallel, because they are related by several side reactions [3]:

$$CH_3OH \leftrightarrow CO + 2H_2 \quad \text{(methanol decomposition)}, \tag{1}$$

$$CH_3OH + H_2O \leftrightarrow CO_2 + 3H_2 \quad \text{(steam reforming)}, \tag{2}$$

$$2CH_3OH \leftrightarrow (CH_3)_2O + H_2O \quad \text{(dehydration)}, \tag{3}$$

$$2CH_3OH \leftrightarrow HCO_2CH_3 + 2H_2 \quad \text{(dehydrogenation)}, \tag{4}$$

$$CO + 3H_2 \leftrightarrow CH_4 + H_2O \quad \text{(methanation)}, \tag{5}$$

$$CO + H_2O \leftrightarrow CO_2 + H_2 \quad \text{(water–gas shift)}, \tag{6}$$

$$2CO \leftrightarrow C + CO_2 \quad \text{(disproportionation)}. \tag{7}$$

* Corresponding author.
E-mail address: mbaeumer@uni-bremen.de (M. Bäumer).
[1] The CRMCN is associated to the Universities of Aix-Marseille II and III.

0021-9517/$ – see front matter
doi:10.1016/j.jcat.2008.02.017

As a consequence of this network of reactions, both CO and CO_2 can occur as products under conditions for methanol decomposition (pure methanol feed) as well as under steam-reforming conditions (methanol and water feed) [5].

From the complexity outlined above arises the need for systematic, mechanistic studies of Pd-based catalysts in the interaction with methanol. Detailed insight into the processes involved can be obtained by a thorough investigation of the interaction of methanol with Pd single crystals [7–9] and, more closely related to real catalysts, with *structurally well-defined* Pd nanoparticles on oxide supports. A powerful approach is to prepare model systems under ultra-high-vacuum (UHV) conditions, in which highly defined metal nanoparticles can be grown on a thin alumina film or other oxide supports by physical vapor deposition (PVD) [10–13]. Detailed investigations of the decomposition of methanol over Pd nanoparticles on Al_2O_3/NiAl(110) have been reported [14–16]. The first steps in methanol decomposition are the formation of methoxy species (adsorbed CH_3O) and subsequent scission of C–H or C–O bonds. C–H bond scission (i.e., dehydrogenation leading to CO) has been found to be the dominant pathway, which can be explained by thermodynamic and kinetic considerations [14]. The rate of C–O bond scission leading to CH_x species and—after further decomposition—finally to atomic carbon was found to be low under UHV conditions but to depend on the type of active site, such as different crystallographic faces, edges and defect sites [14].

A general difficulty of model catalysis under UHV conditions concerns the question of to what extent the detailed information obtained remains meaningful for complex catalysts under real reaction conditions. With respect to methanol decomposition, for example, it was found for Pd(111), as well as for Pd nanoparticles on Al_2O_3/NiAl(110), that C–O bond scission becomes more important at elevated pressure (studied up to ∼15 mbar) and can lead to carbonaceous overlayers and deactivation [14,17–19]. Therefore, it is important to check the transferability of the mechanistic picture obtained under UHV conditions by studying structurally equivalent systems under ambient conditions. With respect to methanol decomposition by Pd-based catalysts, high-quality studies of structurally well-defined systems under ambient conditions are comparably rare. Bertarione et al. investigated the decomposition of methanol over Pd nanoparticles supported on MgO by analyzing adsorbed surface species by FTIR spectroscopy [20]. They found that adsorbed CO species already form at room temperature on the surface as the result of methanol decomposition [20].

In the present work, we address the question of how the decomposition of methanol over Pd-based catalysts can be influenced by adding Co as a second metal to the system. The preparation of *bimetallic* catalysts is a general strategy to modify activity and selectivity [21], and the combination Co–Pd appears relevant here, because bimetallic Co–Pd catalysts have been demonstrated to be interesting in Fischer–Tropsch chemistry [22,23], in which methanol decomposition is a reverse reaction. To obtain detailed mechanistic information and ensure its applicability to realistic reaction conditions, we performed studies of suitable systems under ambient and UHV conditions in a dual approach. Wet-chemically prepared, but structurally well-defined monometallic and bimetallic Co–Pd nanoparticles supported on MgO were used for the investigation of methanol decomposition in the ambient pressure regime. PVD was employed to prepare monometallic and bimetallic nanoparticles on Al_2O_3/NiAl(110) for the studies under UHV conditions. The present article focuses mainly on the particle system studied under ambient conditions; results obtained for the system under UHV conditions are reported in much more detail elsewhere [24].

2. Experimental

Well-defined palladium nanoparticles on magnesium oxide were prepared by wet impregnation of MgO (Fluka, specific surface 30 m^2/g) with palladium acetylacetonate [$Pd(acac)_2$], as described in detail in earlier studies of this system [25] and of similar systems using Pd, Ni, and Cu [26,27]. Bimetallic cobalt-palladium particles on MgO were obtained by an analogous synthesis using $Pd(acac)_2$ and simultaneously $Co(acac)_2$ as precursors for the impregnation procedure. With this technique, the metal composition in the clusters is proportional to the quantities of metal used in the mixture of $Pd(acac)_2$ and $Co(acac)_2$. Monometallic Co nanoparticles on MgO also were prepared for comparison of the reactivity.

TEM investigations were carried out with a Jeol 3010 transmission electron microscope operated at 300 kV. The powders were dropped directly onto the carbon film covering the microscope grid. The supported metal clusters were observed in both top and profile views on the edges of MgO microcubes for the simultaneous determination of the morphology and interface structure and deformations, as in the case of other alloys [28].

IR spectroscopic experiments were performed in diffuse reflection geometry (DRIFTS) with a Biorad FTIR spectrometer (FTS 60A). Samples were pressed into pellets and studied in a reaction cell equipped with a controlled gas supply system, a heating unit, and a photometric detector (Hartmann & Braun URAS 10E) for CO and CO_2 gas analysis at the exit side of the cell. Before measurements, the samples were reduced in the reaction cell under continuous gas flow of ∼50 vol% H_2 in Ar for 1 h at 400 °C. (Successful cleaning of samples that were already exposed to methanol in preceding experiments required several cycles of oxidation and reduction. For oxidative cleaning, pure MgO was exposed to ∼50 vol% O_2 in Ar at 400 °C. For the supported metal catalysts, the oxidation temperature was limited to ∼300 °C. In all cases, the pretreatment was completed by a reduction cycle as described above.)

After the pretreatment, the samples were cooled under continuous Ar or He flow to the required temperatures. Exposure to methanol was realized by directing the feed gas through a methanol reservoir. A condenser maintained at a lower temperature was used to obtain a defined partial pressure. Methanol was carefully purified for the experiments by drying and degassing. The IR spectra were recorded with a resolution of 2 cm^{-1}. All spectra shown herein are referenced to background spectra recorded under pure Ar flow after the H_2 pretreatment.

A laboratory reactor (fixed-bed type, 12-mm diameter) equipped with a controlled gas supply system, heating unit, and photometric CO/CO_2 gas analyzers, was used to study the catalytic performance of the model systems. For the experiments, 10.0 mg of catalyst grains of 0.28–0.45 mm diameter (obtained by sieving crushed pellets) were mixed with 300 mg of quartz grains of 0.4–0.8 mm diameter, to minimize mass transport limitations. This mixture was then placed between quartz wool in the reactor. Before methanol exposure, the samples were reduced inside the reactor under continuous gas flow of ∼50 vol% H_2 in N_2 for 30 min at 300–400 °C. Note that in this context, these temperatures are not sufficient to obtain metallic particles in the case of pure Co [29]. Nonetheless, in what follows, the notation Co/MgO is used.

Methanol was dosed by directing N_2 or He as feed gas through a methanol reservoir and condenser as in the case of the IR spectroscopic experiments. In addition to the photometric detection of CO and CO_2, detailed analysis with gas chromatography was performed in selected cases, using two Agilent 6890 Series gas chromatographs. The first unit was equipped with a thermal conductivity detector (TCD). A 24.5 m, 30 μm Molecular Sieve 5A capillary column was used to separate Ar from O_2, N_2, CH_4, and CO using helium as the carrier gas (adjusted to 37 cm/s at injection time in a constant flow mode). With helium as the carrier gas for solving standard separation problems, the peak area of the H_2 peak cannot be used for quantification, because varying the H_2 content in the sample results in either a positive or a negative peak, or even no peak at all. Therefore, H_2 was analyzed using N_2 as carrier gas. When using N_2 as carrier gas with the Molecular Sieve 5A column, H_2 could be quantified over a large concentration range without problems, whereas the signals from the remaining gases (Ar, O_2, N_2, and CO) were suppressed nearly completely. (The nitrogen flow velocity for these special analyses was reduced to about 28 cm/s, again using the constant flow mode of the instrument.)

The second dual-channel gas chromatograph was equipped with a flame ionization detector (FID) connected to a 50-m × 320-μm column containing a 3-μm SE54 film. This FID with the SE-54 column as "channel A" was used to detect combustible compounds, such as hydrocarbons, ranging from methane (CH_4) up to dodecane ($C_{12}H_{26}$). The carrier gas was He at 38 cm/s at injection time (i.e., 1.40 bar He pressure in constant pressure mode). Channel B was equipped with a TCD, connected to an 80-cm × 3.1-mm stainless steel packed column (60–80 mesh; Molecular Sieve 5A). Helium was used as the carrier gas at 1.8 mL/min in a constant flow mode for the packed column. Using this column, Ar and O_2 were detected as a single peak, whereas N_2, CH_4, CO, and even CO_2 could be separated and quantified. After selecting the optimal GC parameters, both the hydrocarbons and the other gases could be analyzed in a single run on this dual-channel instrument.

Under UHV conditions, monometallic and bimetallic Co–Pd nanoparticles were grown on a thin alumina film, Al_2O_3/NiAl(110), by PVD as described in detail elsewhere [24]. Photoelectron spectroscopy (XPS) and temperature-programmed desorption (TPD) were used to study the interaction of the particle systems with purified methanol. Technical details of the experiments under UHV conditions are reported elsewhere [24].

3. Results and discussion

3.1. Structural characterization of the Me/MgO catalysts

We analyzed structural features of the catalysts by TEM and FTIR spectroscopy of adsorbed CO. Fig. 1 shows overview and high-resolution TEM (HRTEM) images of the monometallic and bimetallic Co–Pd particles on MgO. The particles are highly crystalline, as can be seen from the lattice fringes, and exhibit a face-centered cubic structure. Careful evaluation of the lattice fringes by recording intensity profiles in the HRTEM images [30] revealed a d_{002} spacing of 0.194 ± 0.006 nm for the pure Pd particles. (According to previous HRTEM investigations [30], deviations exist in the first three Pd layers at the interface due to accommodation to the MgO substrate; however, the lattice then relaxes to the bulk value.) In the case of bimetallic particles, local distortions in the disordered fcc structure of the alloy precluded a precise determination of the lattice spacing in the images themselves; therefore, the d_{002} distance was obtained from FFTs calculated from images of selected metal clusters, taking MgO as an internal calibration. In this way, an average value of 0.188 ± 0.009 nm was obtained, which is an intermediate value between pure Pd and pure Co.

According to AAS measurements, the average composition of the bimetallic particles was $Co_{0.59}Pd_{0.41}$. With the help of EDS chemical analysis in electron microscopy using a Jeol 2000 FX microscope, the composition of the particles was first measured at larger scale (i.e., at lower magnifications). Taking the analysis results as an internal calibration, the local composition was determined in 20-nm-diameter areas (corresponding to a selection of about 5–10 individual particles), revealing variations in the Pd content of ±8% around the mean value.

The average particle size was ∼6 nm for the pure Pd particles, ∼4 nm for the bimetallic particles, and ∼4 nm for the pure Co particles. Size histograms are provided in Fig. 1. Note that for all samples, the same total amount (mol) of metal (Pd, Co, or Pd + Co) for a given amount of MgO was used; therefore, the Co and CoPd particles are smaller than the Pd particles.

All of the systems were found to grow in defined epitaxial relations on the support. The (001) face of the particles was parallel to the (001) face of the MgO support, with the [100] axes of the nanoparticles parallel to the [100] axes of the MgO lattice. The shape of the nanoparticles can be described as an octahedron with (111) facets, with the corners truncated by (100) facets. Pd–Co particles observed in profile views along a [100] axis were found to have about the same height:diameter ratio as pure Pd particles ($h/d \approx 0.4$).

The surface of the nanoparticles was characterized by FTIR spectroscopy using CO as a probe molecule. Fig. 2 shows IR spectra after exposure of the samples to 1 mbar CO at room temperature. In the case of Pd/MgO, bands corresponding to CO adsorbed on metallic Pd were observed at 1904, 1983, and 2063 cm^{-1}, which can be assigned to CO in threefold hollow sites, bridge-bonded CO, and linearly bonded CO, re-

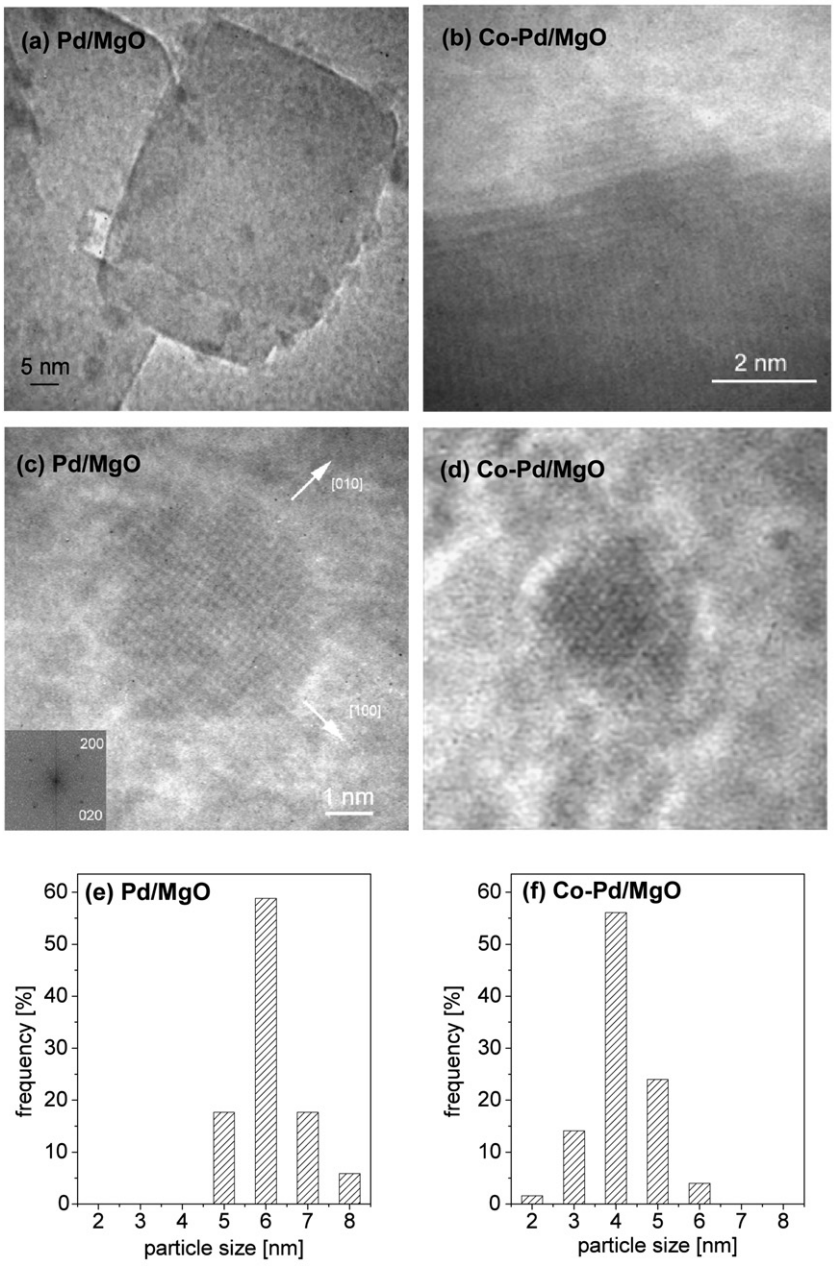

Fig. 1. (a) Overview of pure Pd particles on MgO. (b) HRTEM image of a Co–Pd nanoparticle in profile view on MgO, observed along a [100] direction. (c) High-resolution TEM image of a pure Pd particle observed in top view along a [001] direction. (d) HRTEM image of a Co–Pd nanoparticle in top view on MgO, observed along a [110] direction. (e, f) Histograms of the particle size distribution.

spectively [10–12,14,25,31–36]. Whereas threefold bonded CO occurs only on Pd(111) facets, the band at 1983 cm^{-1} can be assigned to twofold bonded CO on the (100) facets of the Pd particles, according to a recent study by Groppo et al. [36]. Bridge-bonded CO on edges of the Pd crystallites also can contribute to this absorption band [14]. Furthermore, a previous study of the Pd/MgO system showed that linear CO adsorption (band at 2063 cm^{-1}) occurred on Pd atoms at edges of the well-faceted nanoparticles at a CO partial pressure of 1 mbar [25]. The small shoulder at ∼2100 cm^{-1} is assigned to linear CO adsorption on terraces, which plays a minor role under the present experimental conditions [25].

For the bimetallic Co–Pd nanoparticles, three distinct bands were observed in the range corresponding to linear CO adsorption (see Fig. 2b). The bands at ∼2055 and ∼2100 cm^{-1} are due to linear CO adsorption on Pd atoms on edges and terraces, as in the case of the pure Pd nanoparticles [14,25]. The additional band at ∼2081 cm^{-1} can be assigned to a Co carbonyl species [$Co(CO)_n$]. A similar IR band also was observed for Co particles prepared on Al_2O_3/NiAl(110) by PVD and assigned to $Co(CO)_{n=3–4}$ species [37,38]. The assignment is strengthened by the observation that the species can be easily removed by heating to 100 °C (see Fig. 2b), because a similar thermal behavior was found for the Co carbonyl species observed on

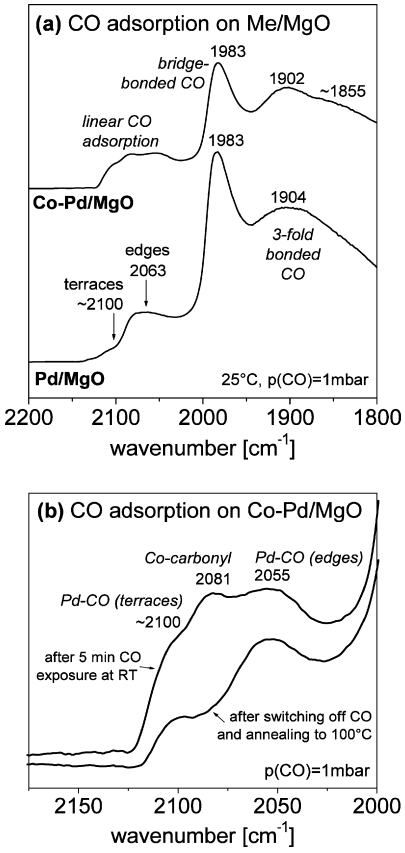

Fig. 2. (a) IR spectra after 5 min exposure of the Pd and Co–Pd nanoparticles on MgO to 0.1 vol% CO in Ar at room temperature. The spectra are referenced to background spectra recorded before CO exposure. (b) Zoom into the spectral region corresponding to linear CO adsorption on the bimetallic particles.

the $Co/Al_2O_3/NiAl(110)$ system [37,38]. For another difference between Pd/MgO and CoPd/MgO, note the appearance of *two* bands in the region corresponding to threefold bonded CO in the case of the bimetallic particles (see Fig. 2a). The second band might be due to CO adsorbed on threefold hollow sites involving both Pd and Co atoms. In conclusion, the analysis of the surface by IR spectroscopy with CO as a probe molecule revealed that Pd and Co atoms are simultaneously present on the surface of the bimetallic nanoparticles.

CO adsorption on Co/MgO did not lead to any pronounced bands in the spectral region of ∼1800–2200 cm^{-1} (spectra not shown). The absence of adsorbed CO species on Co provides an indication that the surface of the pure Co nanoparticles was oxidized and could not be reduced by the applied H_2 pretreatment at 400 °C. Bahlawane et al. studied the reduction of Co_3O_4 with H_2 and observed two transitions in temperature-programmed reduction experiments: Co_3O_4 was reduced to CoO at ∼325 °C, but metallic Co was obtained only at ∼630 °C [29]. Thus, the hydrogen treatment that can be applied in situ at 400 °C is in principle expected to be insufficient to reduce CoO. As can be deduced from the appearance of the Co carbonyl species in the case of the bimetallic Co–Pd nanoparticles, the presence of Pd obviously facilitates the reduction of Co. This is in agreement with studies of Co-based catalysts for the Fischer–Tropsch synthesis in which Pd is used as a promoter metal, facilitating reduction of the catalysts [22,23,39].

Table 1
Determination of the number of surface Me atoms per mg catalyst (the particles were considered as halved cubo-octahedra on the MgO support, and the fraction of surface atoms was calculated using literature models [40])

Sample	wt% Pd (AAS)	wt% Co (AAS)	Particle size (TEM) (nm)	Atoms per particle	Surface atoms (%)	Surface Me atoms per mg catalyst
Pd/MgO	1.30		6.0	3640	22.8	1.7×10^{16}
Co–Pd/MgO	1.72	1.35	4.0	1422	30.6	7.2×10^{16}
Co/MgO		2.02	4.0	1422	30.6	6.3×10^{16}

Because the HRTEM measurements revealed that all of the nanoparticles were of well-defined size and shape, we were able to estimate the number of surface metal atoms per mass unit of the MgO-supported catalysts. For these calculations, the particles were considered halved cubo-octahedra on the MgO support, and statistics developed by van Hardeveld and Hartog were used to determine the fraction of surface atoms [40]. The results are presented in Table 1.

3.2. *Surface species formed on pure MgO in the interaction with methanol*

Before investigating methanol decomposition by the Pd-based catalysts, we studied the interaction of the pure support material with methanol. Fig. 3 shows IR spectra of pure MgO on exposure to 100 mbar methanol at 150 °C (Fig. 3a) and 250 °C (Fig. 3b) as a function of exposure time. At both temperatures, absorption bands developed at the following frequencies after short exposure times: ∼1092, ∼1122, ∼1163 (weak), ∼2595 (weak), ∼2162 (weak), ∼2188 (weak), ∼2806, and ∼2921 cm^{-1}. All of these bands can be assigned to the formation of methoxy species (see also Table 2) [20,41–43]. At 250 °C, additional bands appeared at ∼1603, ∼1630, ∼2727, ∼2847 cm^{-1} and in the region of 1335–1382 cm^{-1}. These bands clearly can be assigned to the development of formate species [20,44–47]. At 150 °C, only very small amounts of formate were observed (weak band at 1603 cm^{-1}).

The development of formates on MgO on methanol exposure remains controversial. In many studies of powder and thin film samples, methoxy species were observed as the only decomposition products of methanol, at least up to ∼300 °C [48–50]. Kondo et al. found formate species as an oxidation product of methoxy groups after also dosing oxygen and heating to 165–230 °C [48]; however, in an early investigation of methanol decomposition on MgO, Kagel and Greenler observed formate formation at 165 °C also in the absence of O_2 [51]. These latter authors suggested that adsorbed methoxy species can react with adjacent OH groups to form formate and hydrogen [51]. To further clarify the situation, we also performed experiments in the presence of small amounts of oxygen; the spectra are compared in Fig. 3c. At 150 °C, the presence of oxygen strongly favored the development of formats; however, at 250 °C, the intensity of the bands corresponding to formate species remained almost unchanged when oxygen was offered. Thus, we can conclude

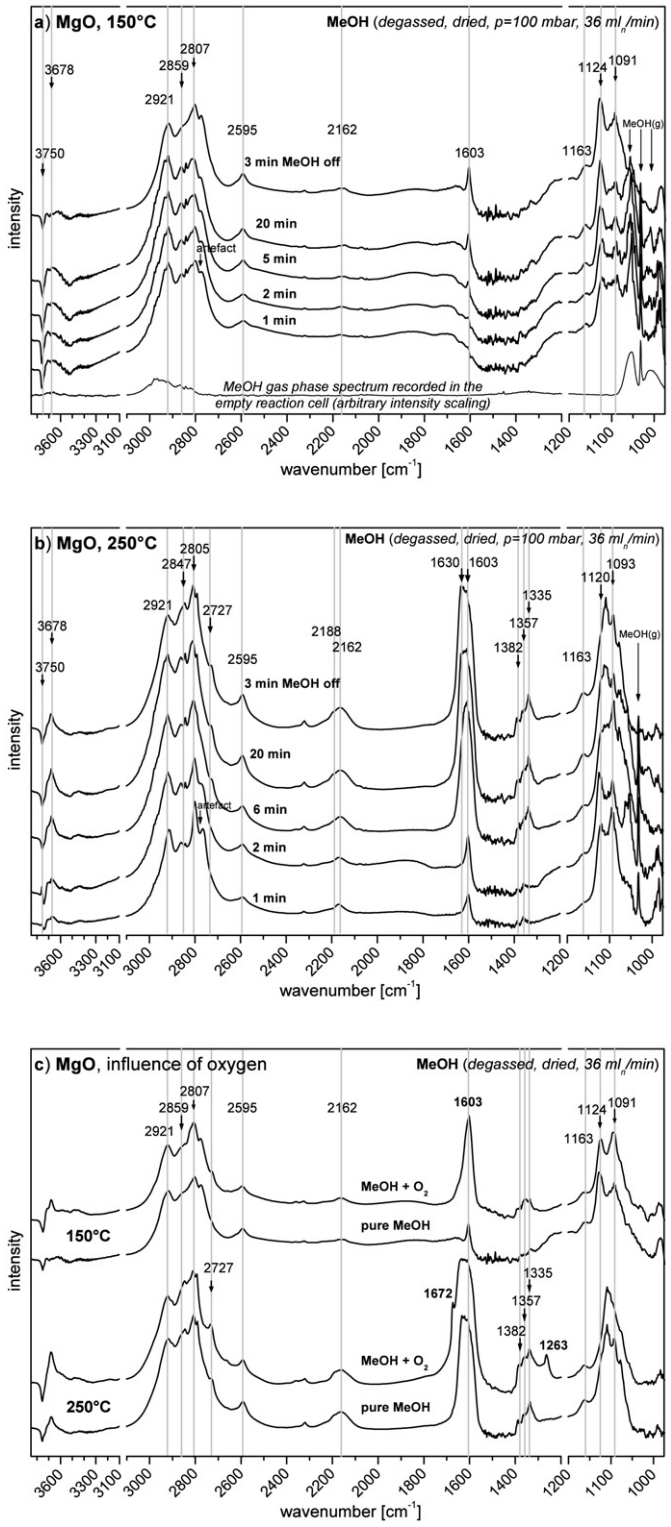

Fig. 3. (a, b) IR spectra after exposure of the pure MgO support to 100 mbar MeOH at 150 °C (a) and 250 °C (b) as a function of exposure time. The spectra are referenced to background spectra recorded at 150 °C (a) and 250 °C (b) before exposure to MeOH. (c) Comparison of spectra after 20 min exposure to 100 mbar MeOH and to a mixture of 40 mbar MeOH and ∼2 mbar O_2. The spectra were recorded 3 min after switching of the reaction gas and are referenced to background spectra recorded before exposure.

that at 250 °C, formates can readily develop in the absence of oxygen, probably by the reaction of methoxy species with OH groups, as suggested by Kagel and Greenler [51]. However, at a lower temperature (150 °C), this mechanism is obviously inhibited, and large amounts of formates develop only in the presence of oxygen.

Along with the dominant features discussed above, several other bands were observed. These are assigned in Table 2.

3.3. Surface species formed on Pd/MgO in the interaction with methanol

Fig. 4a shows an IR spectrum after exposure of the Pd/MgO sample to 100-mbar methanol at room temperature (bottom spectrum in Fig. 4a). An IR band appeared at ∼1841 cm^{-1}, corresponding to threefold bonded CO on Pd [12,20,25], clearly indicating that methanol was dehydrogenated to CO on the Pd/MgO catalyst already at room temperature. Methanol decomposition at room temperature also was observed by Bertarione et al. in a study of structurally less well-defined Pd particles with an average size of ∼11.0 ± 4.5 nm on MgO [20]. In perfect agreement with our data, these authors observed that only the energetically most favorable, threefold hollow sites were occupied by CO at 300 K [20]. But in the present work, other sites on the Pd surface were found to be populated as well, when small amounts of oxygen were offered. In this case, three bands were observed at ∼1835, 1947, and ∼2045 cm^{-1} (upper spectrum in Fig. 4a), which correspond to threefold bonded, bridge-bonded, and linearly bonded CO on Pd, respectively [12,20,25].

This finding can be interpreted as an indication that small amounts of oxygen facilitate the decomposition of methanol at room temperature, and it also reveals mechanistic information: In detail, the band at 2045 cm^{-1} can clearly be assigned to linearly bonded CO on Pd edge atoms [14,25], and the band at ∼1947 cm^{-1} is due to bridge-bonded CO, probably adsorbed on Pd edges as well [14,52]. Therefore, the absence of these bands in the oxygen-free case indicates that the edges of the Pd crystallites are not available for CO adsorption in the absence of oxygen. Studies of methanol decomposition on Pd particles prepared under UHV conditions revealed that carbon and hydrocarbon species resulting from C–O bond scission preferentially decorate the crystallite edges [14,52]; therefore, it is highly likely that the absence of the IR bands at ∼1947 and 2045 cm^{-1} in the oxygen-free case is due to blocking of the crystallite edges by such species resulting from C–O bond scission in our case as well. Thus, the IR spectroscopic experiments provide evidence that C–O bond scission occurs on Pd nanoparticles in the ambient pressure regime as well. Note that CH_x species generated by C–O bond scission were not directly detectable by IR spectroscopy in this study. The expected stretching frequencies for such species [53] are in the region dominated by the intense bands corresponding to methoxy species; therefore, bands corresponding to a minor species cannot be resolved here.

Studies of methanol decomposition on Pd(111) have revealed that oxygen significantly suppresses carbon formation at 300 K [54]. Furthermore, in a study of methanol decomposition

Table 2
Assignment of IR bands (other than carbonyls on Pd) observed after methanol exposure

IR band, wavenumber (cm^{-1})		Assignment	References
This work	Literature		
1037	1050–1060 (ν(C–O))	Molecularly adsorbed MeOH	[20,41,42]
2835	2828–2830	Molecularly adsorbed MeOH	[56,57]
2948	2930–2950	Molecularly adsorbed MeOH	[56,57]
1083–1093	1092–1095 (ν(C–O))	Bridge-bonded methoxy (bonded to 2 Mg^{2+} ions)	[41,42]
1100–1124	1115 (ν(C–O))	Methoxy species (bonded to 1 Mg^{2+} ion)	[41,42]
1163	1165	Methoxy species	[43]
2595, 2162, 2188	2590	Methoxy species (overtones)	[43]
2805–2814, 2921–2930	2805–2824 ($\nu_s(CH_3)$), 2920–2935 ($\nu_{as}(CH_3)$)	Methoxy species	[20]
1328–1384, 1603–1630, 2727–2729, 2847–2865	1340–1390, 1585–1620, 2728–2760, 2820–2840	Formate species	[44–47]
1300–1306, 1507–1550	1300–1370 ($\nu_s(COO^-)$), 1470–1530 ($\nu_{as}(COO^-)$)	Monodentate carbonate[a]	[45]
1240–1263, 1645–1684	1220–1270 (ν_{as}(COO)), 1620–1670 (ν(C=O))	Bidentate carbonate[a] (bonded to 2 metal cations)	[45]
2080	2068	Co carbonyl	[37]

[a] Whereas in the presence of oxygen carbonates can be formed by the interaction of oxygen with adsorbed CO, disproportionation of CO provides a possible explanation for the appearance of carbonates also in the absence of oxygen. In CO adsorption experiments on the same Pd/MgO catalyst a pair of intense bands corresponding to bidentate carbonates was observed at ∼1681 and ∼1215 cm^{-1} at room temperature as the result of CO disproportionation [25].

at higher temperatures (∼450 K) on Pd nanoparticles prepared by PVD, Schauermann et al. reported that carbon species resulting from C–O bond scission can be easily removed from the surface by reaction with adsorbed oxygen [55]. The observation of three IR bands in the presence of small amounts of oxygen indicates that this mechanism for the removal of such species from C–O bond scission also works in the case of Pd catalysts under ambient pressure conditions at room temperature.

Apart from CO adsorbed on Pd, the following surface species were observed at room temperature: An absorption band was detected at ∼1037 cm^{-1}, clearly indicating molecular adsorption of methanol [20,41,42]. Methoxy species also were formed, as indicated by the less-intense band at around ∼1100 cm^{-1}. According to several previous reports [56–58], the frequencies of the bands in the C–H stretching region (2835 and 2948 cm^{-1}) indicate mainly molecular adsorption of methanol, which is in agreement with the dominance of the band at 1037 cm^{-1}. Bands corresponding to formate species were weak at room temperature.

Next, we studied the formation of adsorbed surface species at higher temperatures (150 and 250 °C; see Figs. 4b and 4c). Bands corresponding to CO adsorbed on Pd appeared immediately after contact with methanol. Independent of the presence or absence of oxygen, all types of adsorption sites were immediately populated. Obviously, the blocking of edge sites by carbon species resulting from C–O bond scission is a less-pronounced phenomenon in this temperature range, even in the absence of oxygen. Either the reaction channel for C–O bond scission is suppressed or the higher temperature enhances the probability for the reverse reaction (i.e., recombination of C and O on the surface). We return to this point in Section 3.7.

3.4. Surface species formed on Co–Pd/MgO in the interaction with methanol

Exposure of the bimetallic Co–Pd nanoparticles to pure methanol resulted in the formation of surface species that were basically very similar to those observed for the monometallic Pd/MgO catalyst. As in the case of pure Pd, methanol exposure at room temperature led to the appearance of CO adsorbed on threefold hollow sites as a decomposition product (band at 1855 cm^{-1}). In the presence of oxygen, bridge-bonded CO and linearly bonded CO also were observed. In contrast to Pd/MgO, an additional band was seen at 2080 cm^{-1} in the case of the bimetallic catalysts, demonstrating that in the presence of oxygen at room temperature, methanol decomposition leads also to Co carbonyl species on the surface. This species was not observed at higher temperature (see Figs. 5b and 5c), in agreement with the findings of the CO adsorption experiments (see Section 3.1). Apart from CO species adsorbed on the metal particles, it was again found that methanol adsorbs mainly molecularly at room temperature, whereas methoxy species were observed in the range of 150–250 °C (see Figs. 5b and 5c).

3.5. Surface species formed on Co/MgO in the interaction with methanol

In this work, we could not study the interaction of methanol with pure, metallic Co particles on MgO by IR spectroscopy, because the maximum temperature available for reduction of the catalysts inside the spectrometer's reaction cell was insufficient to obtain metallic cobalt (see also Section 2). According to Bahlawane et al., the cobalt catalyst is expected to be in the state of CoO after reduction with hydrogen at 400 °C [29]. After this pretreatment, no other species than methoxy or formate groups were observed by IR spectroscopy after methanol exposure at temperatures up to 250 °C.

3.6. Catalytic performance of the Me/MgO catalysts for methanol decomposition

We evaluated the catalytic performance with respect to methanol decomposition in the absence and presence of oxygen in a fixed-bed reactor. Before examining the particles supported

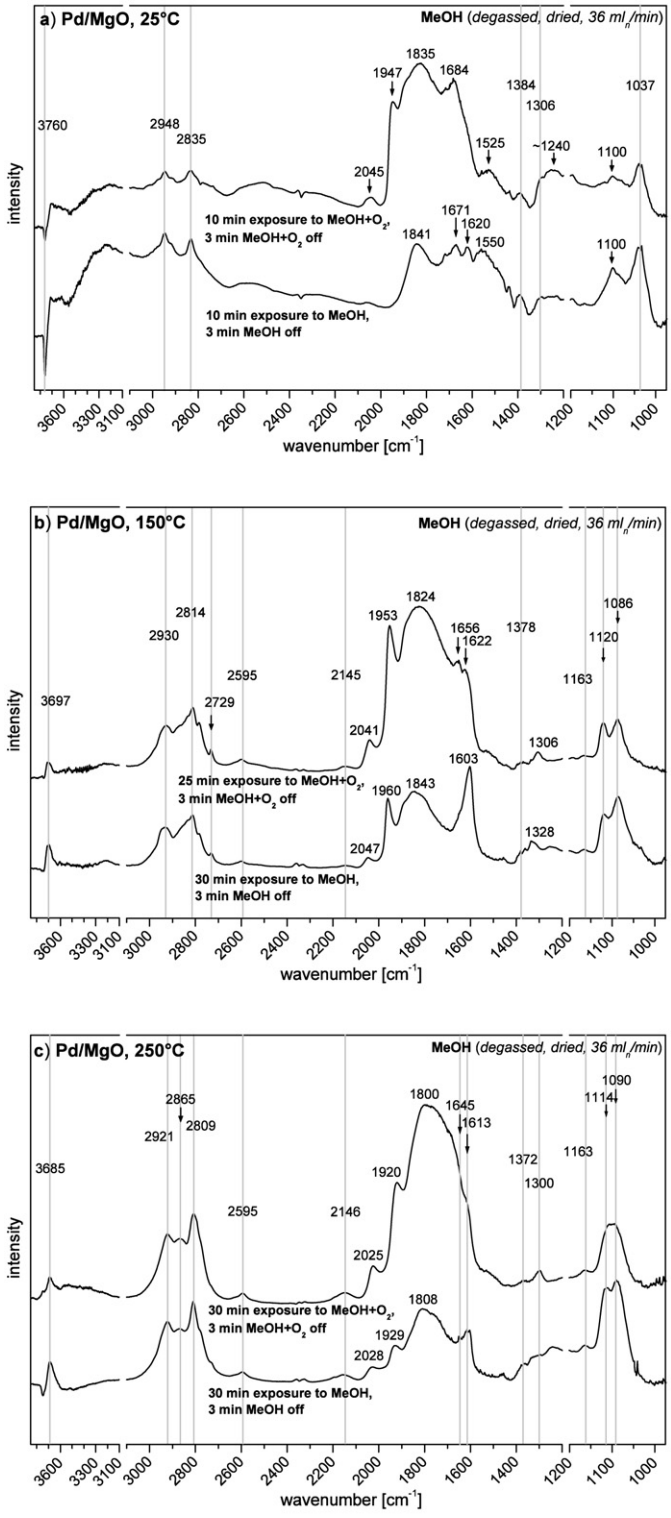

Fig. 4. IR spectra after exposure of Pd/MgO to 100 mbar MeOH and to a mixture of 40 mbar MeOH and ~2 mbar O_2 at 25 °C (a), 150 °C (b), and 250 °C (c). The spectra were recorded 3 min after switching of the reaction gas and are referenced to background spectra recorded before exposure.

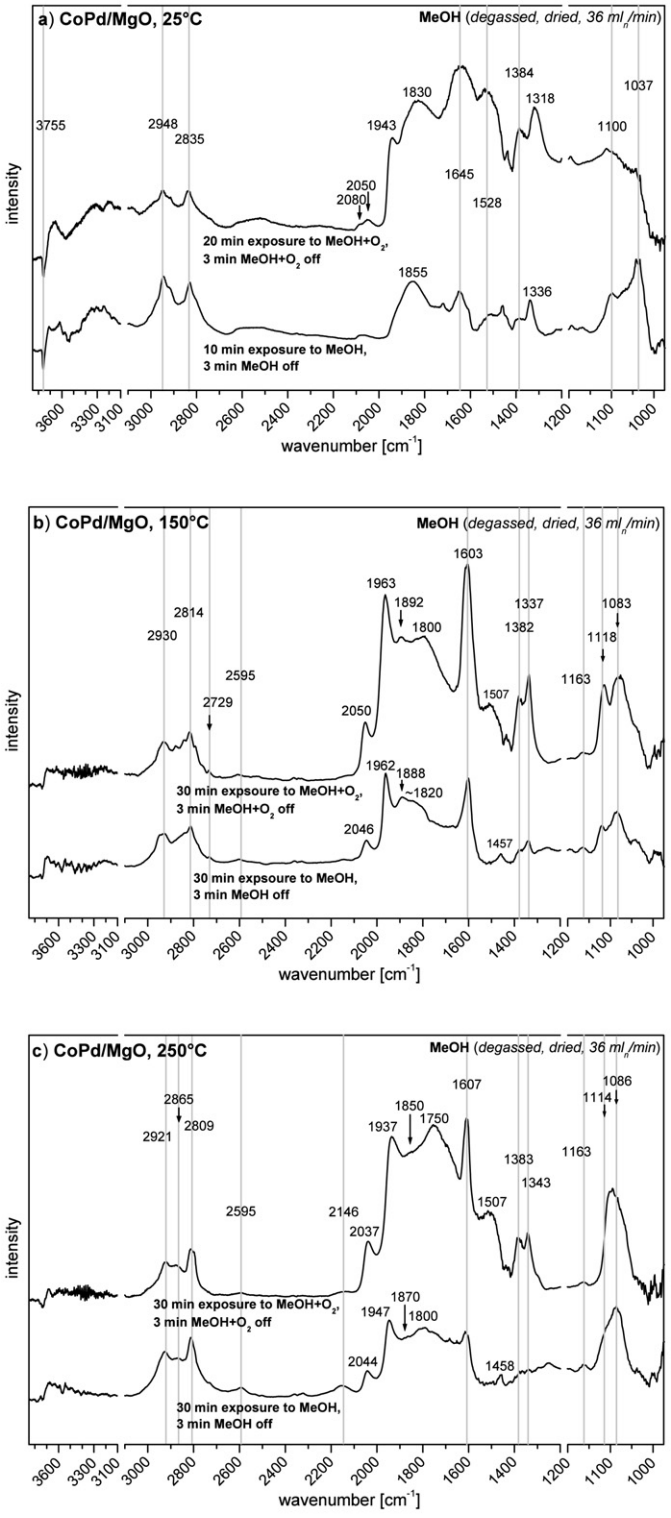

Fig. 5. IR spectra after exposure of CoPd/MgO to 100 mbar MeOH and to a mixture of 40 mbar MeOH and ~2 mbar O_2 at 25 °C (a), 150 °C (b), and 250 °C (c). The spectra were recorded 3 min after switching of the reaction gas and are referenced to background spectra recorded before exposure.

on MgO, we carried out experiments with pure MgO to check whether the support material is completely inactive with respect to methanol decomposition. On exposure to 40 mbar methanol (4 vol%), 0.52 vol% CO was detected at 300 °C when the reactor was loaded with 500 mg of MgO (p.A. quality) (data for lower temperatures: 0.15 vol% CO at 250 °C; ~0 vol% CO at 150 °C). But taking into account that significantly lower amounts of MgO were used in the subsequent

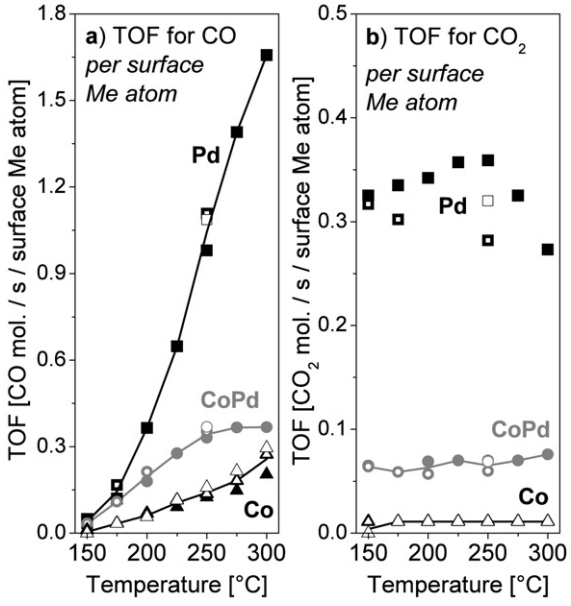

Fig. 6. TOF for CO (a) and CO_2 (b) for Pd/MgO (■), Co–Pd/MgO (●), and Co/MgO (▲) as a function of temperature. Filled symbols (■, ●, ▲) refer to the first cycle, where the temperature was raised. Half-filled symbols (◘, ◎, △) refer to the first cycle, where the temperature was lowered. Open symbols (□, ○, △) refer to the second cycle, where the temperature was raised again. All data points refer to measurements in a steady state which was established ∼30 min after having reached the considered temperature. The partial pressure of MeOH was 40 mbar (in N_2), the partial pressure of oxygen was 5 ± 1 mbar, and the total feed was 35.4 mL_n/min. 10 mg of catalyst with defined grain size were used for the experiments (cf. Section 2).

experiments with the metal particles, this activity can be neglected.

Fig. 6 shows the turnover frequencies (TOFs) for the products CO and CO_2 as a function of temperature as measured in the presence of a small amount of oxygen (i.e., MeOH:O_2 molar ratio of 8:1). Decomposition of methanol to synthesis gas was found to depend strongly on the temperature. Whereas the IR spectroscopic investigations revealed adsorbed CO species already at room temperature on the surface of the Me/MgO catalysts, significant amounts of gas-phase CO were observed only above ∼150 °C (see Fig. 6a). The rate for CO formation per surface Me site was significantly higher for the monometallic Pd particles than for the bimetallic Co–Pd system. Obviously, the addition of Co to the Pd-based catalysts did not have a positive effect with respect to methanol decomposition. For further comparison, we also studied the Co/MgO catalysts. These particles also exhibited activity, but with the lowest TOF. Absolute values of the TOF for CO found for the Pd/MgO catalyst are comparable to those reported at 180 °C for Pd supported on mesoporous ceria–zirconia solid solutions [59]. To study possible activation phenomena, we first heated the samples, then cooled them, and finally reheated them. The results obtained for the different cycles are compared in Fig. 6. The activity increased slightly after the first annealing cycle; however, these effects were not very pronounced. We also studied the long-term stability (data not shown for brevity). Over a period of several hours, the development of CO was stable, and no clear tendencies for further activation or deactivation were evident.

As can be seen in Fig. 6, for all of the Me/MgO catalysts, CO_2 was continuously produced as well in the presence of oxygen. In contrast to CO, the development of CO_2 showed no significant temperature dependence in the range considered. The TOF for CO_2 was ∼5 times higher for the pure Pd particles than for the bimetallic system. The pure Co/MgO catalyst exhibited the lowest rate of CO_2 production.

In the absence of oxygen, the same order was found for the activity of the Me/MgO catalysts. The conversion of methanol to CO was the highest for Pd/MgO and the lowest for Co/MgO. In all cases, however, the TOFs were lower than in the presence of oxygen, but the degree to which the activity was lower depended strongly on the catalyst. Whereas the activity of the Pd/MgO and bimetallic catalysts were lowered by only 15–20% and ∼25%, respectively, in the case of Co/MgO, the TOFs were reduced by ∼75%. CO_2 was not observed in the absence of oxygen. Tests of long-time stability again revealed stable activity on a time scale of several hours (data not shown for brevity).

For the Pd catalyst, along with the photometric detection of CO and CO_2, gas chromatography was used to check for the formation of other products (e.g., methane or formaldehyde). No other products were found independent of the presence or absence of oxygen. In the absence of oxygen, only synthesis gas (H_2 + CO) was produced, and in the presence of oxygen, CO_2 also was detected in the product stream.

3.7. Discussion of the reaction pathways and comparison with the UHV model system

To gain mechanistic insight into the behavior of the Me/MgO catalysts with respect to the methanol decomposition process, we studied in parallel suitable UHV model systems. As reported previously [37,60–62], such systems can be prepared by PVD of Co and Pd on a thin alumina film grown epitaxially on NiAl(110). Small Co nanoparticles (average size ∼2 nm), for example, are obtained through deposition of Co on this support at 300 K [60,61]. When Pd is deposited in a second step on previously prepared Co particles, Pd nucleates on the existing particles, resulting in bimetallic particles with a Co core and a Pd shell. Whether or not the Pd shell completely covers the Co surface depends on the amount of deposited Pd. Up to 1.4 Å Pd on top of 2 Å Co (equivalent layer thickness), the Pd shell is incomplete, and both Co and Pd atoms are present on the surface of the nanoparticles [37], in analogy to the MgO-supported CoPd particles studied under ambient conditions. To obtain pure Pd nanoparticles with structural features similar to those of the Co particles, the deposition temperature must be lowered to 100 K, due to the greater mobility of Pd on the alumina film compared with that of Co [11].

We studied the decomposition of methanol on such model systems using TPD and XPS [24]. We discuss the implications of our findings with respect to the two different pathways of methanol decomposition: the C–H bond scission channel leading to syngas, and the C–O bond scission channel leading first to CH_x species and finally to carbon deposits possibly deactivating the catalysts. Further details of the UHV study are available elsewhere [24].

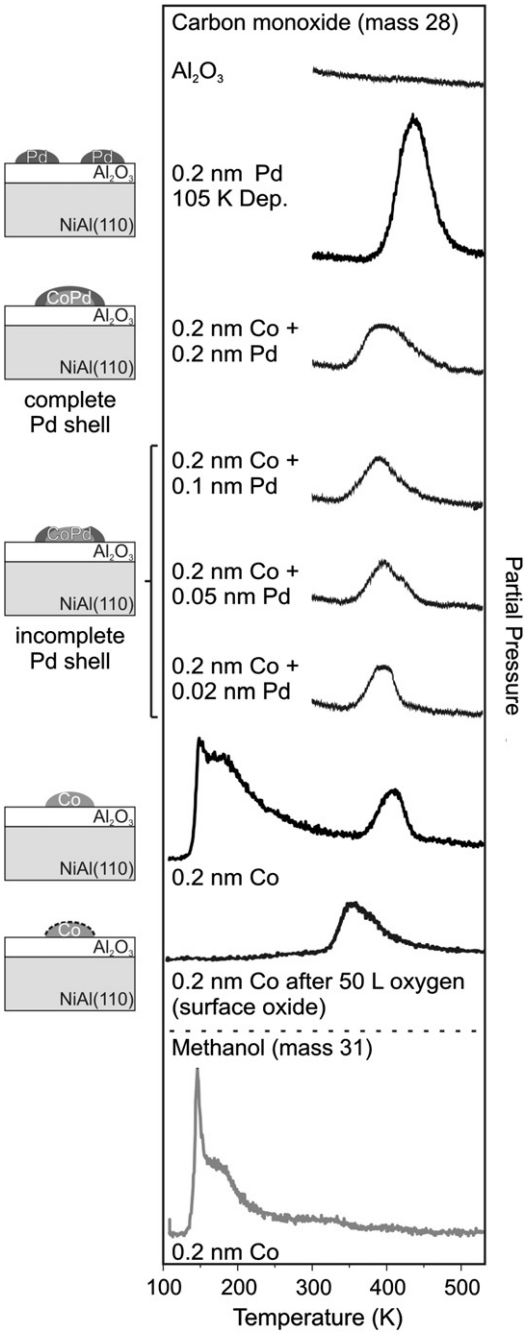

Fig. 7. Temperature-programmed desorption spectra of CO ($m/e = 28$) after exposure of various model catalysts to 20 L methanol at 115 K. A methanol TPD spectrum is included for comparison for monometallic Co particles.

3.7.1. C–H bond scission

Fig. 7 presents TPD spectra recorded after exposing various model systems to 20 L (1 L = 10^{-6} Torr s) methanol at 115 K, which was sufficient to saturate the surface. The particle composition of the respective model systems is schematically depicted on the left side of the figure. The bottom trace shows a TPD spectrum obtained for Co particles at $m/e = 31$, which is representative of the other particles as well. The signals at 150–200 K are due to desorption of physisorbed molecular methanol at low temperatures. In all of the other spectra shown, desorption of CO ($m/e = 28$) was monitored. In all cases, a broad signal was detected at 150–200 K. These signals are due simply to fragmentation of methanol in the mass spectrometer and thus appear concomitantly with desorption of methanol. Yet in all cases, another desorption peak could be observed at higher temperatures (∼130–180 °C [∼400–450 K]), indicating CO formation as a result of methanol decomposition on the nanoparticles. Interestingly, TPD experiments after adsorption of CO revealed a desorption maximum at similar temperatures, pointing to a desorption limitation of CO formation during methanol decomposition. Besides CO, desorption of hydrogen ($m/e = 2$) also was detected, again at temperatures close to the desorption temperatures of adsorbed hydrogen on Pd [63] and Co [64]. Note that no desorption of CO was observed in a reference experiment on the pristine alumina film (upper spectrum in Fig. 7).

The TPD data allow shedding light on two aspects relevant for the C–H scission channel: the onset of catalytic activity and the influence of alloying on activity. Focusing on the onset temperature first, note that the CO desorption temperatures observed for the UHV system are in the temperature range of the onset of methanol conversion to CO under ambient conditions (see Fig. 6a), whereas the IR spectroscopy data presented in Section 3.3 indicated adsorbed CO already at room temperature. Together, these findings suggest that methanol decomposition is desorption-limited under high-pressure conditions as well.

Turning to the catalytic activities and the influence of alloying, the different intensities of the CO desorption peaks in Fig. 7 clearly confirm the lower activity observed for the alloy under ambient pressures compared with pure Pd. At first sight, this is not surprising, given the low intrinsic activity of Co suggested by Fig. 7. Thus, adding Co should reduce the activity, leading to the following sequence: Pd > CoPd > Co. Yet in this context, it is important to note that the activity of the CoPd particles on MgO does not simply reflect the stoichiometrically weighted average of the activities of pure Pd and Co, as clearly shown by the different TOFs in Fig. 6. Above ∼225 °C, the activity of the CoPd particles is significantly lower than the stoichiometrically weighted average. A quantitative evaluation of data collected for various Co–Pd compositions in the UHV experiments demonstrates that the activity of bimetallic particles is nearly independent of the composition [24]. Consequently, the activity of the CoPd catalysts not only is determined by the intrinsic activities of Pd and Co for methanol decomposition, but also is influenced by electronic interactions as a result of the alloying.

Although under ambient conditions, the TOFs for CO are higher for pure Pd than for the bimetallic particles throughout the temperature range studied (see Fig. 6a), these differences are large at high temperatures but become less pronounced near the onset of conversion. In this context, it is interesting to note that according to the TPD results for the UHV model system, the desorption temperature of CO generated via methanol dehydrogenation is lower for the bimetallic particles than for monometallic Pd (∼50 °C) and Co (∼20 °C) particles. This behavior is well known from molecular CO adsorption experiments and can be attributed to the so-called “ligand effect,” that is, electronic interactions of the two metals changing the

binding energy at a given adsorption site [60]. This effect can explain the decreasing gap between Pd and CoPd, because it can be assumed that a facilitated desorption of CO at low temperatures partially compensates for the lower activity of Co sites.

For both the UHV model systems and the metal particles on MgO studied under ambient conditions, the relative positions of Co, CoPd, and Pd within the activity sequence for CO formation are similar. At first sight, this finding is surprising, because the applied reduction treatment for Co/MgO at 400 °C would be expected to be insufficient to obtain metallic Co in a fixed-bed reactor (see Sections 2 and 3.1), whereas the UHV experiments start with metallic Co particles. Thus, to provide a better comparison, we carried out a few reductive pretreatments with H_2 at ∼600 °C in the reactor; however, this did not yield significantly different results with respect to the CO yield. Apparently, regardless of the pretreatment applied, Co reaches an oxidation state under reaction conditions that likely is not fully oxidic and is essentially independent of the initial state. To elucidate this issue with the help of the UHV model system, we performed experiments with Co particles exposed to 50 L of oxygen. In this way, surface and/or subsurface oxygen species are generated, leading to an oxidic adsorption behavior with a CO desorption temperature around 150 K [24,65,66]. The TPD spectrum recorded after methanol exposure, shown in Fig. 7, demonstrates that CO is formed at temperatures only slightly lower than those observed for metallic particles. This finding indicates a concomitant reduction of the particles resulting in a chemical state that is almost metallic. Further experiments with Co particles oxidized to CoO by large doses of oxygen and subsequently exposed to methanol at 525 K confirmed the reduction effect of methanol (data not shown). To which extent remaining oxygen nevertheless exerts some influence on the catalytic behavior of the Co particles cannot be finally clarified on the basis of our findings. In general, the presence of oxygen or oxide phases can dramatically influence the activity of transition metal catalysts [67,68]. As can be inferred from the comparable relative activities found for the Me/MgO catalysts studied under ambient conditions and the metallic particles in the UHV study, the influence of remaining oxygen in the Co/MgO system seems small, however.

3.7.2. C–O bond scission

Apart from the C–H bond scission channel leading to CO and hydrogen, the C–O bond also might be cleaved during the methanol decomposition process [14,17,18,52,55], giving rise to the formation of CH_3 species. The further dehydrogenation of these species leads to carbon deposits (plus oxygen), which may accumulate on the particle surfaces and eventually deactivate the catalysts. On the UHV model systems, combined TPD and XPS experiments indeed revealed that C–O bond scission occurs on both Pd and Co particles, with a greater likelihood of this reaction pathway for Co than for Pd [24]. This finding can be partially ascribed to the ability of Co to dissociate CO resulting from the dominant C–H bond scission channel, thereby increasing the yield of carbon deposits [24]. Studies at elevated pressures (up to ∼15 mbar) further demonstrated for Pd(111), as well as for Pd nanoparticles on Al_2O_3/NiAl(110), that such species finally result in complete deactivation at temperatures up to ∼175 °C [14,17,19].

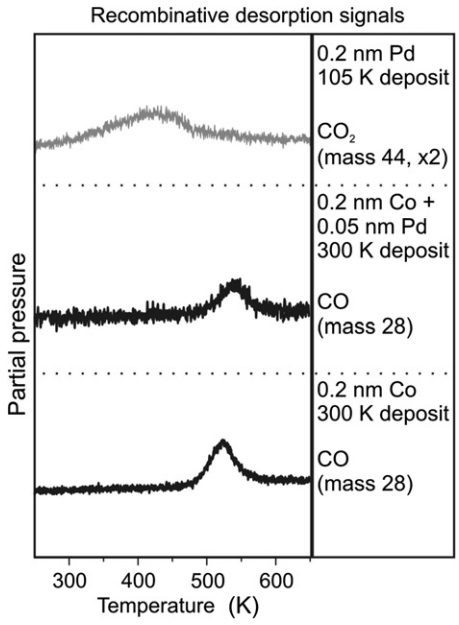

Fig. 8. Temperature-programmed desorption spectra of mono- and bimetallic Me/Al_2O_3/NiAl(110) particles obtained after performing a methanol desorption experiment (i.e. after methanol decomposition) and subsequent exposure to oxygen (1000 L at 300 K). The desorption peaks indicate the recombination of carbon (generated via C–O bond scission) and oxygen to CO_2 (in the case of Pd) and CO (for Co and Co/Pd).

According to these findings, the Pd, Co, and CoPd catalysts investigated in this study should be expected to deactivate rapidly at the high methanol partial pressures applied. As pointed out in Section 3.3, the IR spectroscopy investigations indeed provided evidence for the formation of carbon species at room temperature on the crystallite edges [54]. At higher temperatures (150–250 °C), however, the long-term experiments revealed high steady-state conversion with no signs of deactivation on a time scale of hours (see Section 3.6). Furthermore, in this temperature range, IR spectroscopy revealed no large amounts of carbon on the catalyst surface (see Section 3.3).

As a possible explanation for this phenomenon, Schauermann et al. proposed that the accumulation of carbon species from C–O bond scission is suppressed due to reaction with O (either from the C–O bond scission itself or additionally supplied) [55]. We evaluated this hypothesis using the model catalysts prepared under UHV conditions [24]. For this purpose, Pd, Co, and CoPd particles grown on Al_2O_3/NiAl(110) were first exposed to methanol and heated to ∼230 °C (500 K) to deposit carbon on the surface, and then exposed to a large excess of oxygen at room temperature. Finally, a TPD spectrum was recorded (Fig. 8).

Focusing on Pd first, the detection of a signal corresponding to CO_2 at about 170 °C (∼440 K) provides clear evidence that the reaction of the carbon deposits and adsorbed O on the surface is not kinetically restricted in the temperature range in which catalytic activity was observed. Note that CO_2 instead of CO was formed in the TPD experiment, because oxygen was available in excess and Pd is a good CO oxidation cata-

lyst. In the case of Co and CoPd, recombination also occurred (here leading to CO), but at somewhat higher temperatures. Here, the formation of CO started at ∼210 °C (∼480 K) and reached a maximum at 230–280 °C (∼500–550 K), indicating that removal of the deposits is possible but less facile on these systems.

It is unlikely that the recombination processes described above can lead to a catalyst surface completely free of carbon. Rather, a constant equilibrium concentration of carbon on the catalyst particles under reaction conditions might be expected. The comparison of the experiments performed in the presence and absence of oxygen provides evidence to support this assumption. In the presence of oxygen, higher TOFs were detected (see Section 3.6). This can be explained by the carbon deposits, the coverage of which is reduced in the presence of small amounts of oxygen in the feed due to increased recombination and oxidation.

In this context, it is conspicuous that the promotional effect of oxygen is most pronounced for Co, suggesting that the steady-state concentration of carbon is highest on these particles. This is of course in agreement with the less-facile recombination and the higher tendency for carbon formation compared with Pd (see above). Along with the lower intrinsic activity of Co, the higher carbon concentration also likely contributes to the low activity of Co catalysts in syngas formation and the diminishing effect of Co in the bimetallic system.

4. Summary and conclusions

In the present study, we investigated the decomposition of methanol over monometallic and bimetallic Co/Pd catalysts. Structurally well-defined catalysts for experiments in UHV and at ambient pressure were studied in a dual approach. Controlled deposition of organometallic precursors on MgO was used to obtain Me/MgO catalysts for studies in the ambient pressure regime. PVD on Al_2O_3/NiAl(110) was chosen to prepare well-defined model systems under UHV conditions.

Comparative studies revealed that methanol is decomposed to CO already at room temperature, but with the reaction limited by desorption of CO from the surface. Temperatures above ∼150 °C are required for high steady-state conversion. The addition of cobalt does not improve the reaction rate, although Co lowers the enthalpy of adsorption of CO by an electronic effect (ligand effect).

Ranking the activities of all monometallic and bimetallic particle compositions studied, the same order was found for both types of systems, the Me/MgO catalysts and the model catalysts prepared under UHV conditions: Pd > CoPd > Co. Although in the case of pure Co, the initial state under ambient conditions likely was CoO, results obtained with the UHV model system suggest that methanol can significantly reduce the catalyst under reaction conditions.

In all of the systems studied, methanol was found to decompose via two reaction pathways, a dominant C–H bond scission channel leading to H_2 and CO (syngas) and the less likely C–O bond scission channel leading to carbon deposits and oxygen on the catalyst surface. These species decrease the activity for syngas formation but do not induce full deactivation. This effect is related to the fact that carbon formed can be removed by recombination with O at the relevant reaction temperatures. Under reaction conditions, probably a steady-state concentration of carbon species exists on the particle surfaces. In the case of Co, this equilibrium concentration is higher due to the greater likelihood of C–O bond scission and a less effective recombination process. The higher carbon coverage likely contributes to the Co catalysts' low activity for syngas formation, in combination with the lower intrinsic activity compared with Pd.

We also studied the effect of small amounts of oxygen on methanol decomposition over the Me/MgO catalysts. Oxygen was found to enhance the activity, allowing more effective removal of carbon deposits by oxidation to CO or CO_2. This effect of oxygen is more pronounced for the Co-containing catalysts, for which the recombination process is less effective.

Acknowledgments

This work was supported by the German Research Foundation (DFG) within the priority program SPP 1091 and by an individual grant, as well as by the Fonds der Chemischen Industrie. Yu.B. received a fellowship from the Alexander von Humboldt Foundation. The authors are grateful for fruitful discussions with Prof. Dr. G. Rupprechter (TU Vienna), Prof. Dr. J. Libuda (University Erlangen), and Dr. Th. Risse (FHI, Berlin).

References

[1] J.L.G. Fierro, M.A. Pena, in: J.A. Anderson, M. Fernandez Garcia (Eds.), Supported Metals in Catalysis, Imperial College Press, London, 2005.
[2] S. Hara, W.-C. Xu, K. Sakaki, N. Itoh, Ind. Eng. Chem. Res. 38 (1999) 488.
[3] Y. Liu, T. Hayakawa, T. Ishii, M. Kumagai, H. Yasuda, K. Suzuki, S. Hamakawa, K. Murata, Appl. Catal. A 210 (2001) 301.
[4] W.-J. Shen, Y. Matsumura, Phys. Chem. Chem. Phys. 2 (2002) 1519.
[5] N. Iwasa, N. Takezawa, Top. Catal. 22 (2003) 215.
[6] Y. Suwa, S. Ito, S. Kameoka, K. Tomishige, K. Kunimori, Appl. Catal. A 267 (2004) 9.
[7] R.J. Levis, J. Zhicheng, N. Winograd, J. Am. Chem. Soc. 111 (1989) 4605.
[8] M. Rebholz, N. Kruse, J. Chem. Phys. 95 (1991) 7745.
[9] F. Solymosi, A. Berko, Z. Toth, Surf. Sci. 285 (1993) 197.
[10] C.R. Henry, Surf. Sci. Rep. 31 (1998) 231.
[11] M. Frank, M. Bäumer, Phys. Chem. Chem. Phys. 2 (2000) 3723.
[12] M. Bäumer, H.-J. Freund, Prog. Surf. Sci. 61 (1999) 127.
[13] H.-J. Freund, Surf. Sci. 500 (2002) 271.
[14] M. Bäumer, J. Libuda, K.M. Neyman, N. Rösch, G. Rupprechter, H.-J. Freund, Phys. Chem. Chem. Phys. 9 (2007) 3541.
[15] S. Schauermann, J. Hoffmann, V. Johánek, J. Hartmann, J. Libuda, H.-J. Freund, Catal. Lett. 84 (2002) 209.
[16] J. Hoffmann, S. Schauermann, V. Johánek, J. Hartmann, J. Libuda, J. Catal. 213 (2003) 176.
[17] M. Morkel, V.V. Kaichev, G. Rupprechter, H.-J. Freund, I.P. Prosvirin, V.I. Bukhtiyarov, J. Phys. Chem. B 108 (2004) 12955.
[18] V.I. Bukhtiyarov, V.V. Kaichev, I.P. Prosvirin, Top. Catal. 32 (2005) 3.
[19] M. Borasio, O. Rodriguez de la Fuente, G. Rupprechter, H.-J. Freund, J. Phys. Chem. B 109 (2005) 17791.
[20] S. Bertarione, D. Scarano, A. Zecchina, V. Johanek, J. Hoffmann, S. Schauermann, J. Libuda, G. Rupprechter, H.-J. Freund, J. Catal. 223 (2004) 64.
[21] C.T. Campbell, Surf. Sci. Rep. 27 (1997) 1.

[22] L. Guczi, Z. Schay, G. Stefler, F. Mizukami, J. Mol. Catal. A 141 (1999) 177.
[23] L. Guczi, L. Borko, Z. Schay, D. Bazin, F. Mizukami, Catal. Today 65 (2001) 51.
[24] T. Nowitzki, H. Borchert, B. Jürgens, T. Risse, V. Zielasek, M. Bäumer, Chem. Phys. Chem., in press.
[25] H. Borchert, B. Jürgens, V. Zielasek, G. Rupprechter, S. Giorgio, C.R. Henry, M. Bäumer, J. Catal. 247 (2007) 145.
[26] S. Giorgio, C. Chapon, C.R. Henry, Langmuir 13 (1997) 2279.
[27] S. Sao Joao, S. Giorgio, C.R. Henry, C. Chapon, S. Bourgeois, J.M. Penisson, J. Phys. Chem. B 109 (2005) 342.
[28] S. Giorgio, C.R. Henry, Microsc. Microanal. Microstruct. 8 (1997) 379.
[29] N. Bahlawane, E.F. Rivera, K. Kohse-Höinghaus, A. Brechling, U. Kleineberg, Appl. Catal. B 53 (2004) 245.
[30] S. Giorgio, C. Chapon, C.R. Henry, G. Nihoul, Philos. Mag. B 67 (1993) 773.
[31] H. Unterhalt, G. Rupprechter, H.-J. Freund, J. Phys. Chem. B 106 (2002) 356.
[32] T. Lear, R. Marshall, J.A. Lopez-Sanchez, S.D. Jackson, T.M. Klapötke, M. Bäumer, G. Rupprechter, H.-J. Freund, D. Lennon, J. Chem. Phys. 123 (2005) 174706.
[33] S. Bertarione, D. Scarano, A. Zecchina, V. Johanek, J. Hoffmann, S. Schauermann, M.M. Frank, J. Libuda, G. Rupprechter, H.-J. Freund, J. Phys. Chem. B 108 (2004) 3603.
[34] K. Wolter, O. Seiferth, H. Kuhlenbeck, M. Bäumer, H.-J. Freund, Surf. Sci. 399 (1998) 190.
[35] I.V. Yudanov, R. Sahnoun, K.M. Neyman, N. Rösch, J. Hoffmann, S. Schauermann, V. Johánek, H. Unterhalt, G. Rupprechter, J. Libuda, H.-J. Freund, J. Phys. Chem. B 107 (2003) 255.
[36] E. Groppo, S. Bertarione, F. Rotunno, G. Agostini, D. Scarano, R. Pellegrini, G. Leofanti, A. Zecchina, C. Lamberti, J. Phys. Chem. C 111 (2007) 7021.
[37] A.F. Carlsson, M. Bäumer, T. Risse, H.-J. Freund, J. Chem. Phys. 119 (2003) 10885.
[38] T. Risse, A. Carlsson, M. Bäumer, T. Klüner, H.-J. Freund, Surf. Sci. 546 (2003) L829.
[39] J. Zhang, J. Chen, Y. Li, Y. Sun, J. Nat. Gas Chem. 11 (2002) 99.
[40] R. van Hardeveld, F. Hartog, Surf. Sci. 15 (1969) 189.
[41] M.-L. Bailly, C. Chizallet, G. Costentin, J.-M. Krafft, H. Lauron-Pernot, M. Che, J. Catal. 235 (2005) 413.
[42] M. Bensitel, O. Saur, J.C. Lavalley, Mater. Chem. Phys. 28 (1991) 309.
[43] T. Ito, T. Watanabe, T. Tashiro, K. Toi, J. Chem. Soc. Faraday Trans. 85 (1989) 2381.
[44] M.A. Babaeva, D.S. Bystrov, A.Yu. Kovalgin, A.A. Tsyganenko, J. Catal. 123 (1990) 396.
[45] A.A. Davydov, Infrared Spectroscopy of Adsorbed Species on the Surface of Transition Metal Oxides, John Wiley & Sons, Chichester, 1990.
[46] D.G. Rethwisch, J.A. Dumesic, Langmuir 2 (1986) 73.
[47] K. Teramura, T. Tanaka, H. Ishikawa, Y. Kohno, T. Funabiki, J. Phys. Chem. B 108 (2004) 346.
[48] J. Kondo, Y. Sakat, K. Maruya, K. Tamaru, T. Onishi, Appl. Surf. Sci. 28 (1987) 475.
[49] S.H.C. Liang, I.D. Gay, Langmuir 1 (1985) 593.
[50] C. Di Valentin, A. Del Vitto, G. Pacchioni, S. Abbet, A.S. Wörz, K. Judai, U. Heiz, J. Phys. Chem. B 106 (2002) 11961.
[51] R.O. Kagel, R.G. Greenler, J. Chem. Phys. 49 (1968) 1638.
[52] S. Schauermann, J. Hoffmann, V. Johanek, J. Hartmann, J. Libuda, H.-J. Freund, Angew. Chem. Int. Ed. 41 (2002) 2532.
[53] J. Rasko, J. Bontovics, F. Solymosi, J. Catal. 143 (1993) 138.
[54] M. Borasio, Ph.D. thesis, University of Berlin, Berlin, 2006.
[55] S. Schauermann, J. Hoffmann, V. Johanek, J. Hartmann, J. Libuda, Phys. Chem. Chem. Phys. 4 (2002) 3909.
[56] J. Rudberg, M. Foster, J. Phys. Chem. B 108 (2004) 18311.
[57] C. Di Valentin, A. Del Vitto, G. Pacchioni, S. Abbet, A. Wörz, K. Judai, U. Heiz, J. Phys. Chem. B 106 (2002) 11961.
[58] S.E. Collins, M.A. Baltanas, A. Bonivardi, Appl. Catal. A 295 (2005) 126.
[59] M.P. Kapoor, A. Raj, Y. Matsumura, Microporous Mesoporous Mater. 44–45 (2001) 565.
[60] M. Heemeier, A.F. Carlsson, M. Naschitzki, M. Schmal, M. Bäumer, H.-J. Freund, Angew. Chem. Int. Ed. 41 (2002) 4073.
[61] A.F. Carlsson, M. Naschitzki, M. Bäumer, H.-J. Freund, J. Phys. Chem. B 107 (2003) 778.
[62] A.F. Carlsson, M. Naschitzki, M. Bäumer, H.-J. Freund, Surf. Sci. 545 (2003) 143.
[63] S.K. Shaikutdinov, M. Frank, M. Bäumer, S.D. Jackson, R.J. Oldman, J.C. Hemminger, H.-J. Freund, Catal. Lett. 80 (2001) 115.
[64] K. Habermehl-Cwirzen, K. Kauraala, J. Lahtinen, Phys. Scr. T 108 (2004) 28.
[65] T. Nowitzki, V. Zielasek, M. Bäumer, in: Proceedings of the 10th German–Vietnamese Seminar, in: Springer Proceedings in Physics, in press.
[66] T. Nowitzki, A.F. Carlsson, O. Martyanov, M. Naschitzki, V. Zielasek, T. Risse, M. Schmal, H.-J. Freund, M. Bäumer, J. Phys. Chem. C 111 (2007) 8566.
[67] F. Solymosi, Catal. Rev. 1 (1968) 233.
[68] S. Penner, D. Wang, B. Jenewein, H. Gabasch, B. Klötzer, A. Knop-Gericke, R. Schlögl, K. Hayek, J. Chem. Phys. 125 (2006) 094703.